

Sediment flux from a mountain belt derived by landslide mapping

Niels Hovius*

Department of Earth Sciences, University of Oxford, Parks Road, Oxford OX1 3PR, United Kingdom

Colin P. Stark

Géosciences, Université de Rennes, Campus de Beaulieu, 35042 Rennes, France

Philip A. Allen*

Department of Earth Sciences, University of Oxford, Parks Road, Oxford OX1 3PR, United Kingdom

ABSTRACT

In humid uplands landsliding is the dominant mass wasting process. In the western Southern Alps of New Zealand landslides are scale invariant and have a power-law magnitude frequency distribution. Independent studies from other regions suggest that this is a general property of landsliding. This observation is of critical importance to the evaluation of the impact of events of different length scales over different time intervals on landscape evolution. It is particularly useful when estimating regional geomorphic rates, because it constrains the frequency and overall significance of extreme events, which cannot otherwise be evaluated. By integrating the complete response of the system, we estimate the regional denudation rate due to landsliding to be $9 \pm 4 \text{ mm yr}^{-1}$. Sediment discharge from the western Southern Alps is dominated by landslide-derived material.

INTRODUCTION

Landscape evolution arises from the integrated effect of erosion and mass transfer over geologic spatial and temporal scales. In many humid uplands landscape evolution is dominated by landsliding across a wide range of length scales (Anderson, 1994; Gerrard, 1994; Greenbaum et al., 1995; Schmidt and Montgomery, 1995; Burbank et al., 1996). A great body of work documents the morphology and mechanics of individual instances of slope instability, but few studies have considered the process at a larger scale. Furthermore, direct observations of the long-term role of landsliding are lacking. Extrapolating short-term geomorphic observations to time scales pertinent to landscape development requires an understanding of the scaling behavior of the processes involved, in particular the magnitude and frequency with which they occur (Wolman and Miller, 1960). Magnitude-frequency studies require a broad range of spatial and temporal constraints and a large number of observations. These three conditions are met in the central section of the western Southern Alps of New Zealand, where we have obtained a 60 yr record of landsliding from multiple sets of air photos. This data set has enabled us to quantify the rates and scaling of landsliding and the concomitant mass fluxes.

STUDY REGION

The Southern Alps are a linear, asymmetric mountain belt marking the oblique compressional boundary between the Australian and the Pacific plate (Walcott, 1978). Rock uplift rates approach-

ing 7 mm yr^{-1} (Bull and Cooper, 1986; Tippett and Kamp, 1993; Simpson et al., 1994) have assisted the building of 2 to 4 km of relief, which forms a barrier across the prevailing, moisture laden, northwest winds moving off the Tasman Sea. Mean annual precipitation rates reach as much as 15 m on the steep western flank of the orogen (Griffiths and McSaveney, 1983a). Here, dissected, rectilinear slopes, frequently steeper than 45° and with thin (<1 m) regolith cover, have formed in zones of schists and gneisses trending parallel to the range bounding Alpine fault. Dense, natural, temperate rain forests prevail below a tree line at $\sim 1200 \text{ m}$ altitude. These conditions are very favorable to the occurrence of rapid mass wasting. The principal hillslope erosion processes are landslides, involving falls, slumps and slides, predominantly displacing bedrock, and debris flows (definitions according to Varnes, 1978).

LANDSLIDE MAPPING

The availability of multiple sets of air photos for the central Southern Alps, for the period between 1948 and 1986, allows assessment of the distribution of landsliding both in space and time (Hovius, 1995). The study region is enclosed by the Waitaha River and the Moeraki River, the western coastline of South Island, and the main divide of the Southern Alps (Fig. 1). This region comprises 13 transverse catchments draining the central segment of the Southern Alps toward the west and their downstream continuation across a narrow coastal plain. Two series of air photos (1964/65, 1:16 500; 1985/86, 1:50 000) provide complete coverage of the study region. Additional coverage of the coastal plain and the frontal part of the mountain belt is available for

the intermediate period (1972/73, 1:25 000; 1980/81, 1:25 000). For the area north of the Karangarua River time coverage includes the series of 1948 (1:15 840). In all, 2640 photos were inspected in a regional reconnaissance of highly inaccessible terrain. Approximate dates of erosional events were established by comparing photographic coverage made at intervals.

Recent landslides can be discerned on air photos using morphometric criteria and high surface reflectivity. Reflectivity contrasts between vegetated and nonvegetated zones fade as erosion scars are recolonized by vegetation, thus adding a distinction between recent and subrecent events. In the nival zone, where vegetation is absent, such discrimination is impossible. The present reconnaissance is therefore limited to the lower, vegetated parts of the mountain belt, below $\sim 1400 \text{ m}$ altitude.

All landslide scars and debris flows identified on the air photos were mapped on 1:50 000 scale topographic maps, where available, and on 1 in:1 mi maps for the remaining parts of the region (both map series: Department of Survey and Land Information, Wellington, New Zealand) and were subsequently digitized. As a rule, only scars or deposits without second-growth vegetation were included. In the remainder of this paper we discuss landslide scars only. The areas of individual landslides observed in the study region range from 100 m^2 to about 1 km^2 . Mapping resolution was primarily determined by the scale of the maps; in this study it is reasonable to assume a maximum mapping accuracy of 1.5 mm, which is equivalent to 75 m on a 1:50 000 scale map. The effective mapping range therefore has a lower limit of $5 \times 10^{-3} \text{ km}^2$. Simultaneous field-

*Present address: Department of Geology, Trinity College, Dublin 2, Ireland.

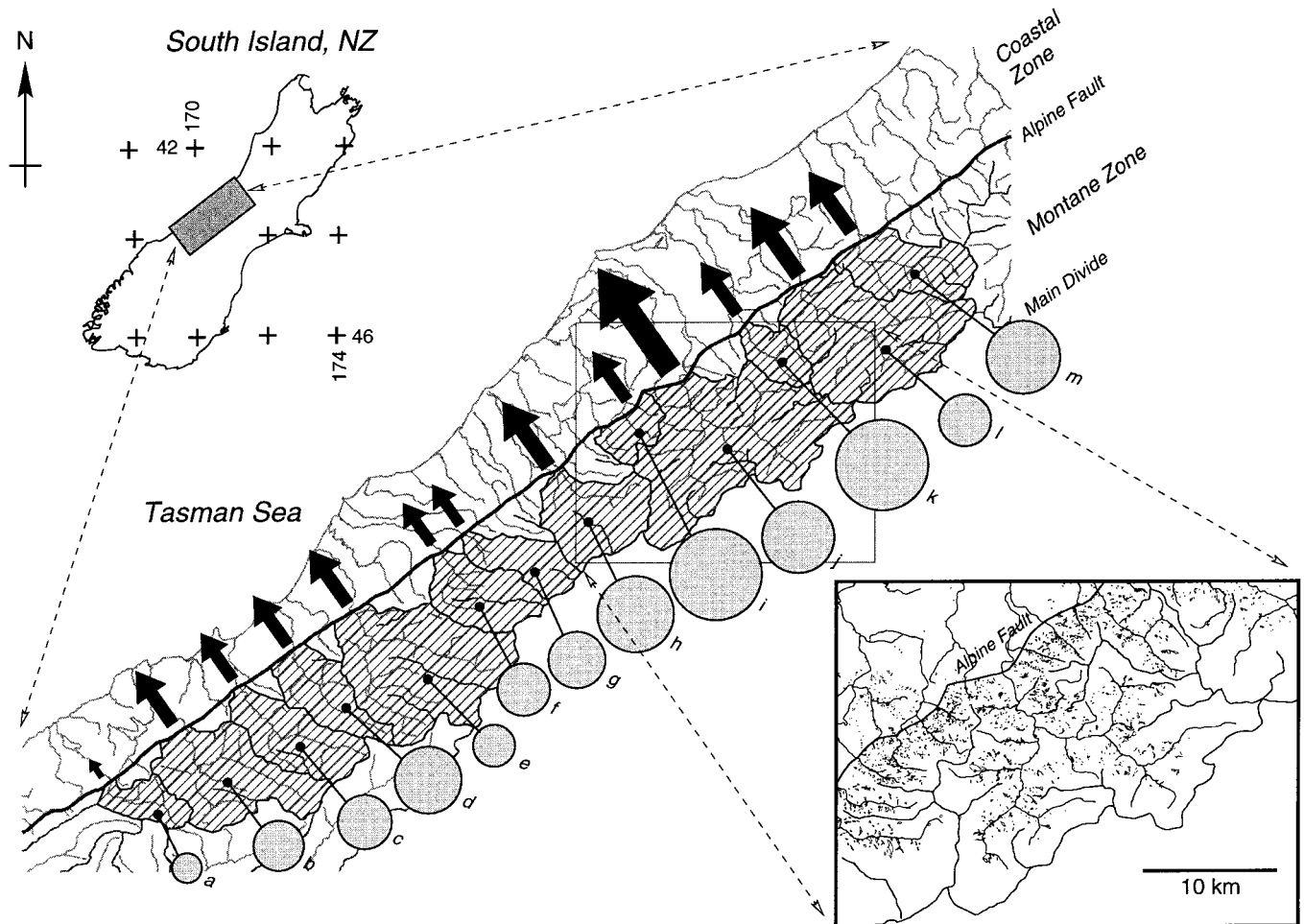


Figure 1. Overview of denudation rates and sediment discharges from 13 catchments draining western side of Southern Alps, calculated from 60 yr landslide record. Inset shows section of landslide data base, covering montane part of Whataroa catchment, flanked by Poerua and Waitangitaona basins. Denudation rates (E) and sediment discharges (D) are indicated respectively by circles and arrows, the areas of which are proportional to each estimate, and are listed as follows: (a) Moeraki: $E = 1.8 \text{ mm yr}^{-1}$ ($D = 1.2 \times 10^5 \text{ m}^3 \text{ yr}^{-1}$); (b) Paringa: $E = 5.5 \text{ mm yr}^{-1}$ ($D = 1.3 \times 10^6 \text{ m}^3 \text{ yr}^{-1}$); (c) Mahitahi: $E = 6.3 \text{ mm yr}^{-1}$ ($D = 9.8 \times 10^5 \text{ m}^3 \text{ yr}^{-1}$); (d) Makawhio: $E = 9.9 \text{ mm yr}^{-1}$ ($D = 1.1 \times 10^6 \text{ m}^3 \text{ yr}^{-1}$); (e) Karangarua: $E = 3.7 \text{ mm yr}^{-1}$ ($D = 1.3 \times 10^6 \text{ m}^3 \text{ yr}^{-1}$); (f) Cook: $E = 5.8 \text{ mm yr}^{-1}$ ($D = 7.9 \times 10^5 \text{ m}^3 \text{ yr}^{-1}$); (g) Fox: $E = 7.5 \text{ mm yr}^{-1}$ ($D = 7.1 \times 10^5 \text{ m}^3 \text{ yr}^{-1}$); (h) Waiho: $E = 12.2 \text{ mm yr}^{-1}$ ($D = 2.0 \times 10^6 \text{ m}^3 \text{ yr}^{-1}$); (i) Waitangitaona: $E = 18.1 \text{ mm yr}^{-1}$ ($D = 1.1 \times 10^6 \text{ m}^3 \text{ yr}^{-1}$); (j) Whataroa: $E = 11.4 \text{ mm yr}^{-1}$ ($D = 5.1 \times 10^6 \text{ m}^3 \text{ yr}^{-1}$); (k) Poerua: $E = 18.1 \text{ mm yr}^{-1}$ ($D = 1.2 \times 10^6 \text{ m}^3 \text{ yr}^{-1}$); (l) Wanganui: $E = 6.1 \text{ mm yr}^{-1}$ ($D = 2.1 \times 10^6 \text{ m}^3 \text{ yr}^{-1}$); (m) Waitaha: $E = 11.6 \text{ mm yr}^{-1}$ ($D = 1.7 \times 10^6 \text{ m}^3 \text{ yr}^{-1}$).

work in several catchments in early 1994 validated the mapping technique. Most scars predating 1973 were overgrown with shrubs, whereas younger scars supported little second-growth vegetation. Thus the temporal resolution of the mapping method was found to be ~ 20 years.

Following the method we have outlined, we generated a map of the distribution of landslides on the western flank of the central Southern Alps and the adjacent coastal plain (Fig. 1). This region has a total surface area of 4970 km^2 , 2670 km^2 of which are vegetated montane terrain and therefore mappable. In all, 7691 landslides were mapped, representing between 40 and 60 years of mass wasting, depending on the location.

Landslide density is clearly higher in the Alps or montane zone compared to the coastal zone, with an abrupt increase at the range bounding Alpine fault. Because the two zones have important topographic, climatologic, and geologic differences, their landslide inventories should not be

combined. In this study we have therefore focused on the distribution of landslides in the montane zone.

MAGNITUDE AND FREQUENCY

The mapped areas of all 4984 observed landslides in the montane zone east of the Alpine fault exhibit a magnitude-frequency distribution (Fig. 2) that can be described by a power law over the approximately two orders of area magnitude for which reliable measurements are available. This distribution may be written in a cumulative form,

$$n_c(A \geq A_c) = \kappa(A_c/A_r)^{-\beta} A_r, \quad (1)$$

where $n_c(A \geq A_c)$ is the number of slides per year of magnitude greater than or equal to A_c over a reference area A_r , κ is the rate of landsliding per unit area per year, and β is a dimensionless scaling exponent. We define $A_r = 1 \text{ km}^2$, and obtain the best fit power law model (1) by linear regres-

sion over the restricted, but most robust, data range from 10^{-2} km^2 to 10^{-1} km^2 . As Figure 2 shows, the gradient of the log-log form of the model is $\beta = 1.16$, and the intercept at $A = A_r$ is $\kappa = 5.4 \times 10^{-5} \text{ km}^{-2} \text{ yr}^{-1}$.

A similar scale-invariant distribution (Turchette, 1992) of landslide-magnitude frequency has been observed by Fuyii (1969) in a sample of about 650 rainfall-induced events from upland areas of Japan. For magnitudes ranging between 10^{-3} km^2 and 10^{-1} km^2 , Fuyii found that $\beta = 0.96$. Sugai et al. (1994) conducted a more extensive study in the Akaiishi Mountains of central Japan. Rather than considering the magnitude of landslide scars, they measured the area of individual landslide deposits, discarding all observations smaller than 10^{-2} km^2 . Their results indicate a power law distribution of landslide-magnitude frequency over an area scale range of less than one order of magnitude, with a regional value of β of ~ 1.0 . Given independent observations of

power law scaling behavior from three regions, it seems that scale invariance is a general property of landslides, although differences exist between fitted model parameters.

VOLUMETRIC ANALYSIS

In order to estimate the total volume of material eroded by landsliding we need to quantify the geometry of the landslides as well as their size distribution. We have found the mean plan form of Southern Alps landslides to be approximately elliptical with an aspect ratio of about 2.0 across all length scales. As the inset in Figure 2 shows, the minor axis length (width) of the landslide is roughly equal to the square root of its area, $l \approx \sqrt{A}$, so that we can rewrite equation 1 using this width measure:

$$n_c(l \geq l_c) = \kappa l_c^{-2\beta} \quad (2)$$

Landslide width, rather than length, is chosen as the equivalent length scale because its relationships with respect to both landslide area and thickness are more tightly constrained in our data set. Field studies (Ohmori, 1992; Hovius, 1995) suggest a linear width-depth scaling relation for mean slide thickness t :

$$t(l) = \epsilon l \quad (3)$$

Cross sections of several larger landslide scars in the montane area yield an estimate for ϵ of 0.05 ± 0.02 . The landslide volume discharge at length scale l is therefore given by

$$v(l) = n(l)A(l)t(l) = \epsilon l^3 n(l), \quad (4)$$

where $n(l)$ is the number distribution of landslides of length l , derived from the cumulative distribution of equation 2 by $n(l) = dn_c / dl$. The total volume of landslide material yielded from the reference area A_r is then

$$V = 2\beta \epsilon \kappa \int_{L_0}^{L_1} l^{2-2\beta} dl, \quad (5)$$

where L_1 is the maximum possible width of a landslide in the region and L_0 is the minimum. From this follows the very important conclusion that when $\beta < 1.5$ and $L_1 \gg L_0$, as is the case in the Southern Alps, denudation due to landsliding is dominated by the largest events. Then we obtain

$$V \approx \frac{2\beta \epsilon \kappa}{(3-2\beta)} L_1^{3-2\beta} \quad (6)$$

The upper length scale for landsliding in the region, L_1 , is not precisely determined. The largest observed event has a width of ~1 km and an area of 1 km², but the dimensions of the longest valley sides would allow for the occurrence of events of well over 2 km. Because no relicts of such larger events have been identified in the postglacial landscape, we consider $L_1 \approx 1$ km. Using $\kappa = 5.4 \times 10^{-5}$ km⁻² yr⁻¹ for the 2670 km² mapped mon-

tane zone, we obtain an estimate for the denudation rate due to landsliding of the western Southern Alps of 9 ± 4 mm yr⁻¹.

Assuming that the observed scaling behavior is a general characteristic of landslides throughout the region, local landsliding rates may be determined using data from each catchment over the size range of 10⁻² km² to 10⁻¹ km², for which equation 1 produces the most robust fit. Using equation 6, these local values of κ were converted into estimates of denudation rate, shown as circles in Figure 1. Most drainage basins were found to have denudation rates between 5 mm yr⁻¹ and 12 mm yr⁻¹, although higher rates were observed in two small basins at the range front. These denudation rates were then integrated over the surface area of each catchment to obtain local annual sediment discharges, shown as arrows in Figure 1. Discharges range from 1×10^6 m³yr⁻¹ to 2×10^6 m³yr⁻¹, with a peak value of 5×10^6 m³yr⁻¹ for the Whataroa catchment. These simple estimates are open to refinement, by a more sophisticated length-depth scaling relation for slides, and by a more precise definition of the maximum length scale on which sliding can occur. However, the relative proportions of catchment-wide denudation rates and sediment discharges will remain unaffected because both

these factors are likely to vary little between drainage basins. An added requirement for extrapolation of denudation estimates beyond the period covered by the airphoto record is a well constrained relation between the rate of landsliding and the probability distribution of climatic and seismic triggers.

Denudation estimates may be compared with rates calculated from sediment discharge measurements for some streams along the Alpine fault, which range from 4.7 to 11.9 mm yr⁻¹. The two principal rivers in the region, the Hokitika to the north, and Haast to the south of the study region, have basin-wide denudation rates of 6.3 and 4.7 mm yr⁻¹, respectively (calculated from specific sediment yields listed in Griffiths, 1979). Denudation rates in the Waitangitona catchment were estimated by Griffiths and McSaveney (1986) to be 4.6 ± 0.3 mm yr⁻¹, from a 17 yr deposition record on the alluvial fan at the range front. Measurements from Ivory basin, a partially glaciated cirque basin in the upper part of the Waitaha basin, give a five year average denudation rate of 5.5 ± 0.3 mm yr⁻¹ (Hicks et al., 1990). In the nearby nonglaciated Cropp basin a three-year study (Griffiths and McSaveney, 1983b) yielded a denudation rate of 11.0 ± 0.9 mm yr⁻¹. As there is little intramontane storage of eroded

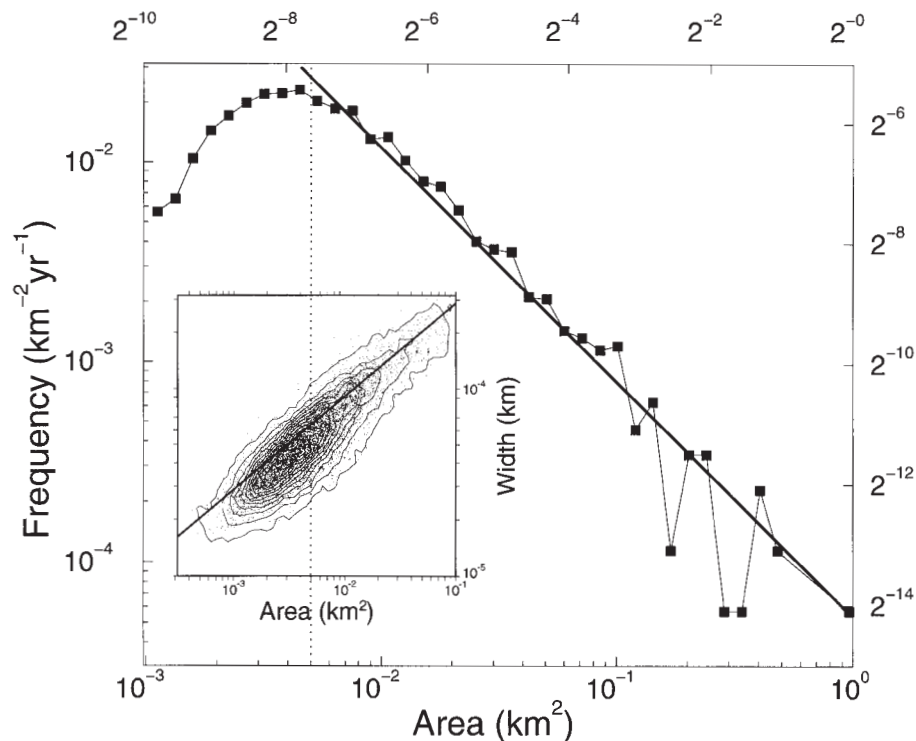


Figure 2. Size distribution of mapped landslides in central western Southern Alps. Main graph is histogram employing logarithmic bin widths ($\log 2w = 1/4$). Mapping method puts lower bound of reliable frequency estimates at about 5×10^{-3} km², which is indicated (for both graphs) by vertical dashed line. Above this cutoff, very clear power law trend is observable over two orders of length scale magnitude. Straight line indicates best fit power law model, where gradient is equal to exponent β in equation 1. Correctly normalized, this curve describes probability density function of landsliding of certain magnitude at given time. Inset graph illustrates relationship between landslide area and width of best fit ellipse. This relation is employed in volumetric analysis (equations 3–6). Kink in histogram may be mapping artifact or reflection of size discontinuity in mass wasting mechanics.

material, correspondence of these rates with denudation rates estimated from landslide mapping indicates that bedrock landsliding accounts for most material that leaves the mountain belt, and that, at present, other erosion processes are of subsidiary importance to the orogenic mass budget of the Southern Alps.

CONCLUSIONS

Magnitude-frequency distributions of mass wasting processes may be derived from time series of remotely sensed images, or, given time constraints on the regeneration of vegetation, from single sets of images. We have documented the magnitude-frequency distribution of landslides in the Western Southern Alps of New Zealand using air photos covering a time span of 40 years. This distribution can be fit with an analytic expression, here a power law, which must be integrated over the entire scale range of the process to arrive at long-term hillslope-erosion rates. Comparison of our volumetric estimates with downstream sediment loads indicates that erosion of the western Southern Alps occurs principally through bedrock landsliding. The slope of the observed landslide-size frequency distribution demonstrates that the bulk of the erosional work is done by high-magnitude low-frequency events.

ACKNOWLEDGMENTS

This study was supported by a British Council Fellowship to Niels Hovius, Natural Environment Research Council Postdoctoral Research Fellowship GT4/F/91/GS/3 to Colin Stark, and grants from Stichting "Het Fonds van Jan de Koning" and Stichting "VSB Fonds." We thank Kitti van Ramshorst for her assistance with data processing, and gratefully acknowledge access to the DOSLI photo archive in Hokitika. Bob Anderson and Dave Montgomery have provided stimulating reviews.

REFERENCES CITED

- Anderson, R. S., 1994, Evolution of the Santa Cruz Mountains, California, through tectonic growth and geomorphic decay: *Journal of Geophysical Research*, v. 99, p. 20161–20179.
- Bull, W. B., and Cooper, A. F., 1986, Uplifted marine terraces along the Alpine fault, New Zealand: *Science*, v. 234, p. 1225–1228.
- Burbank, D. W., Leland, J., Fielding, E., Anderson, R. S., Brozovic, N., Reid, M. R., and Duncan, C., 1996, Bedrock incision, rock uplift and threshold hillslopes in the northwestern Himalayas: *Nature*, v. 379, p. 505–510.
- Fuyii, Y., 1969, Frequency distribution of the magnitude of the landslides caused by heavy rain-fall: *Seismological Society of Japan Journal*, v. 22, p. 244–247.
- Gerrard, J., 1994, The landslide hazard in the Himalayas: Geological control and human action: *Geomorphology*, v. 10, p. 221–230.
- Greenbaum, D., and 10 others, 1995, Rapid methods of landslide hazard mapping: Papua New Guinea case study: *British Geological Survey Technical Report WC/95/27*.
- Griffiths, G. A., 1979, High sediment yields from major rivers of the Western Southern Alps, New Zealand: *Nature*, v. 282, p. 61–63.
- Griffiths, G. A., and McSaveney, M. J., 1983a, Distribution of mean annual precipitations across some steep-land regions of New Zealand: *New Zealand Journal of Science*, v. 26, p. 197–209.
- Griffiths, G. A., and McSaveney, M. J., 1983b, Hydrology of a basin with extreme rainfalls—Cropp River, New Zealand: *New Zealand Journal of Science*, v. 26, p. 293–306.
- Griffiths, G. A., and McSaveney, M. J., 1986, Sedimentation and river containment on Waitangitanga alluvial fan—South Westland, New Zealand: *Zeitschrift für Geomorphologie*, v. 30, p. 215–230.
- Hicks, D. M., McSaveney, M. J., and Chinn, T. J. H., 1990, Sedimentation in proglacial Ivory Lake, Southern Alps, New Zealand: *Arctic and Alpine Research*, v. 22, p. 26–42.
- Hovius, N., 1995, Macro scale process systems of mountain belt erosion and sediment delivery to basins, [Ph.D. thesis]: Oxford, United Kingdom, University of Oxford, 232 p.
- Ohmori, H., 1992, Morphological characteristics of the scar created by large-scale rapid mass movement, *Japanese Geomorphological Union Transactions*, v. 13, p. 185–202.
- Schmidt, K. M., and Montgomery, D. R., 1995, Limits to relief: *Science*, v. 270, p. 617–620.
- Simpson, G. D. H., Cooper, A. F., and Norris, R. J., 1994, Late Quaternary evolution of the Alpine Fault Zone at Paringa, South Westland: *New Zealand Journal of Geology and Geophysics*, v. 37, p. 49–58.
- Sugai, T., Ohmori, H. and Hirano, M., 1994, Rock control on magnitude-frequency distribution of landslide: *Transactions of the Japanese Geomorphological Union*, v. 15, p. 233–351.
- Tippett, J. M., and Kamp, P. J. J., 1993, Fission track analysis of the late Cenozoic vertical kinematics of continental Pacific crust, South Island, New Zealand: *Journal of Geophysical Research*, v. 98, p. 16119–16148.
- Turcotte, D. L., 1992, *Fractals and chaos in geology and geophysics*: Cambridge, United Kingdom, Cambridge University Press, 221 p.
- Varnes, D. J., 1978, Slope movement and types of processes, *in* Schuster, R. L., and Krizek, R. J., eds., *Landslides*: Washington, D.C., Analysis and control: Transportation Research Board Special Report 176, National Academy of Sciences, p. 11–33.
- Walcott, R. I., 1978, Present tectonics and late Cenozoic evolution of New Zealand: *Royal Astronomical Society Geophysical Journal*, v. 52, p. 137–164.
- Wolman, M. G., and Miller, J. P., 1960, Magnitude and frequency of forces in geomorphic processes: *Journal of Geology*, v. 68, p. 54–74.

Manuscript received June 24, 1996

Revised manuscript received November 4, 1996

Manuscript accepted November 18, 1996